I&EC research
Industrial & Engineering Chemistry Research

pubs.acs.org/IECR
Article

Facilitated Transport Nanocomposite Membranes for CO_2/H_2 Separation: The Effect of Mobile Carriers

Wenqi Xu, Arne Lindbråthen, Xueru Wang, Zhongde Dai, and Liyuan Deng*

Cite This: *Ind. Eng. Chem. Res.* 2023, 62, 15202−15211

ABSTRACT: Using CO_2-selective membranes based on facilitated transport mechanisms has been reported as an energy-efficient approach for hydrogen purification from CO_2-containing mixed gas streams. In this work, four CO_2-philic mobile carriers, i.e., guanidine-based and amino acid-based salts, were introduced to a facilitated transport nanocomposite membrane to enhance the CO_2/H_2 separation performance. The effects of the types and loading of mobile carriers on the CO_2 permeation properties were studied. Mechanisms that lead to enhanced CO_2 transport by mobile carriers in the facilitated transport membrane matrix and nanofiller−polymer interfaces are discussed. With an optimized loading of the selected mobile carriers, the AspK-based membrane doubled the CO_2 permeance without sacrificing the selectivity, while the ProK-based membrane increased the CO_2/H_2 selectivity by 25% with a marginally increased CO_2 permeance. The optimized membranes show separation performances far above the upper bound of the CO_2/H_2 upper bound.

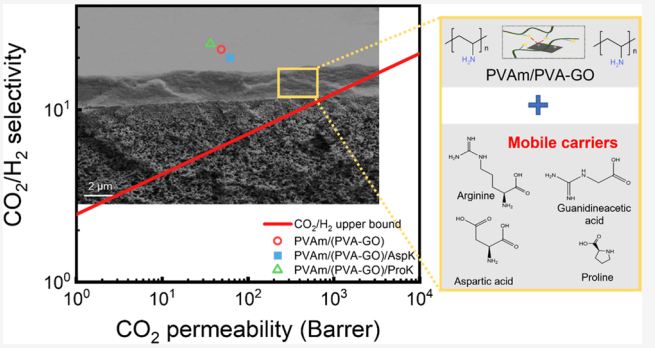

1. INTRODUCTION

The increasing CO_2 level in the atmosphere is believed to be the most direct cause of climate change.[1] One of the major sources of CO_2 emission is fossil fuel-based energy generation, for example, using coal and natural gas.[2] Thus, the global energy structure can be shifted to noncarbon-based fuels, such as H_2, to reduce CO_2 emissions and overcome climate challenges.

Hydrogen is an excellent and promising energy carrier, and the most common source of H_2 is from syngas through the integrated gasification combined cycle (IGCC) using fossil fuels. In recent years, in accordance with a net-zero future, more research regarding H_2 production has been shifting to renewable and sustainable resources, such as biofuels,[3] including the conversion of waste biomass through dark fermentation to produce biohydrogen.[4] The H_2 gas streams from both H_2 production routes contain CO_2 and H_2 in the mixtures saturated with water. However, H_2 produced from IGCC is under elevated temperature and pressure,[5] while the fermentative biohydrogen is under relatively mild conditions at near ambient pressure and temperatures.[4]

The CO_2 and H_2 separation is the key to obtaining high-purity H_2 as a pure fuel. Traditional CO_2 and H_2 separation methods, like pressure swing adsorption (PSA) and absorption, need either an additional step to remove water vapor from the water-saturated gas streams or extra energy for solvent/sorbent regeneration. A gas separation membrane is a promising alternative to traditional CO_2 separation technologies considering membranes' high modularity, small footprint, no chemical emissions, and easier up-scaling.[6] Moreover, using membranes is more economical for small- to medium-sized plants such as a fermentative H_2 production process.

There are two types of membranes for CO_2 and H_2 separation, namely, H_2-selective membranes and CO_2-selective membranes. H_2-selective membranes have been extensively studied, including palladium membranes, polymeric membranes, and carbon membranes,[7] but only a few CO_2-selective membranes have been investigated because the molecular diameter of H_2 (2.9 Å) is much smaller than that of CO_2 (3.3 Å);[8] it is hard to control a larger molecule to transport quicker than a smaller one. Polymeric membranes with very high CO_2-sorption selectivity can be an option, but a "trade-off", also called the Robeson upper bound, between selectivity and gas permeability[9,10] generally limits polymeric membranes' gas separation performance.[11]

One approach to developing high-performance membrane materials to overcome the "trade-off" between gas permeability and selectivity is through the smart design of facilitated transport-based membranes, for instance, to enable CO_2 transport through a more efficient reversible reactive pathway

Received: July 14, 2023
Revised: August 16, 2023
Accepted: August 23, 2023
Published: September 5, 2023

https://doi.org/10.1021/acs.iecr.3c02400
Ind. Eng. Chem. Res. 2023, 62, 15202−15211

in addition to the solution-diffusion path.[12] Typically, the reactive carriers are amino groups fixed to the backbone of the polymer chains, also called fixed-site carriers (FSC), such as the amino groups in polyvinylamine (PVAm) and poly(allylamine) (PAAm), which also reversibly react with CO_2 in the presence of water to increase the level of CO_2 permeation. It is worth noting that the reactions between CO_2 and CO_2-reactive groups of carriers usually require the presence of water,[13] so there is no need for an additional step to remove water from the gas streams.

Our previous work reported a nanocomposite FSC membrane for its good CO_2/H_2 selectivity, in which poly(vinyl alcohol)-modified graphene oxide (PVA-GO) was embedded in a PVAm membrane to enhance CO_2 transport but introducing a barrier effect against the more diffusive smaller molecules, i.e., H_2. Although PVAm has the highest content of primary amino groups in all polymers,[14] the amino groups are locked to the backbones. Nevertheless, the amine-based polymer chains may become more flexible with increased distance when in a water-swollen state, leading to better CO_2-carrier accessibility in the membrane matrix. Moreover, based on process simulation studies on the use of CO_2-selective membranes for CO_2/H_2 separation,[15] the performance of the PVAm/PVA-GO membrane should be further improved to make the process more economical and thus competitive with other commercially available technologies.

As an effective approach, small CO_2-philic molecules, called mobile carriers, are often incorporated into FSC membranes to provide additional CO_2 carriers and hence to improve the CO_2 permeation properties, such as by increasing the mobility of amine groups and providing more active CO_2 carrier sites. In fact, the added small CO_2-philic molecules increase the density of CO_2-reactive groups in the membrane, making the CO_2 transport more competitive compared with that of H_2 and combating the carrier saturation phenomena (i.e., the reaction sites are saturated). In a nanocomposite membrane containing two-dimensional (2D) nanofillers (such as the PVAm/PVA-GO membrane), mobile carriers are also expected to be enriched around the GO interfaces, adding extra affinity to CO_2 transport along the GO−polymer interface, competing with H_2. Dai et al. reported a facilitated transport membrane using amino acid salts as mobile carriers with successfully increased CO_2 permeance for CO_2/N_2 separation.[16] Janakiram et al. prepared ionic liquid (1-ethyl-3-methylimidazolium acetate)-based membranes for CO_2/N_2 separation, resulting in a CO_2 permeance increase of approximately 87% compared with a neat membrane matrix.[17] Ho and coworkers reported introducing 2-aminoisobutyric acid-potassium salt as a mobile carrier into PVA-based cross-link membranes, resulting in superior CO_2/H_2 separation performance under a high temperature of ≥100 °C.[18]

Alkalines, amines, and amino acid salts based on primary amine groups have been widely reported as mobile carriers in facilitated transport membranes.[16−18] Similar to these mobile carriers, guanidine and its derivatives are also efficient CO_2 absorbents in the form of zwitterions when in the presence of water, leading to reversible interaction between CO_2 and guanidino groups.[19] Nevertheless, few papers reported using guanidine and guanidine derivatives as mobile carriers.

In this work, based on the literature study, two guanidine-based salts (arginine-based potassium salt (ArgK) and guanidine acetic acid-based potassium salt (GuaK)) and two amino acid salts (aspartic acid-based potassium salt (AspK) and proline-based potassium salt (ProK)) were selected and introduced to PVAm/(PVA-GO) membranes as mobile carriers to further enhance the CO_2 permeance. The addition of these four mobile carriers may also potentially increase the CO_2/H_2 selectivity due to the high reaction rate constant.[20] The chemical structures of the selected mobile carriers are shown in Figure 1.

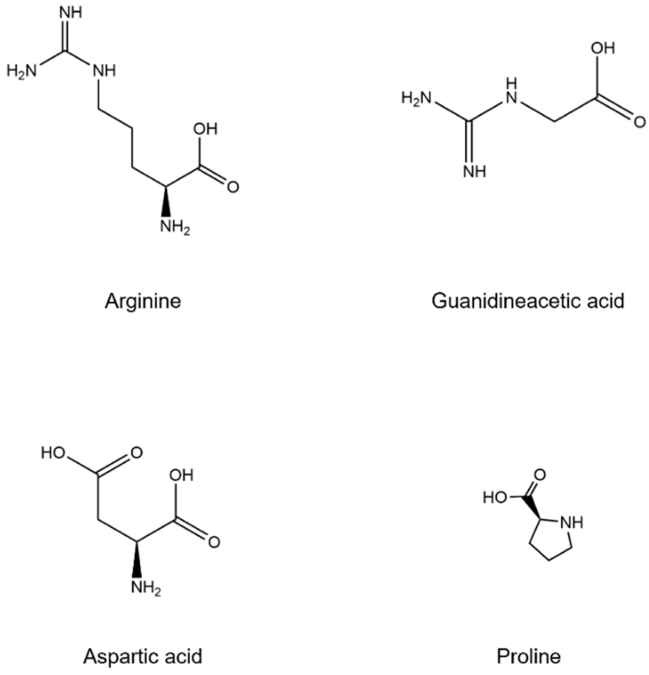

Figure 1. Chemical structure of guanidine-based and amino acid-based molecules.

As can be seen, the chain length, contents of amine groups, and tightness of the structure of these salts are different. For example, two amino acid-based molecules (aspartic acid and proline) have a more loosened structure with shorter chains than guanidine-based ones, while the guanidine-based molecules (arginine and guanidine acetic acid) contain a higher concentration of amine groups but show a more bulky structure. These differences in mobile carriers are expected to bring different effects to the membrane performances.

In this work, the effects of mobile carrier types and their loadings were studied and discussed. Optimized membranes were determined according to the resulting improvement in CO_2/H_2 separation performances. Membrane materials were characterized to evaluate their chemical and physical properties by scanning electron microscopy (SEM), Fourier transform infrared (FTIR) spectroscopy, and thermogravimetric analysis (TGA). The gas separation tests of all of the membranes were measured under ∼100% relative humidity conditions. The effect of the temperature on gas separation performance was also studied to determine optimal process conditions.

2. MATERIALS AND METHODS

2.1. Materials. Lupamin 9095 was received from BASF AG Germany. Poly(vinyl alcohol) (PVA, M_w: 85,000−124,000, 87−89% hydrolyzed), sodium hydroxide (NaOH, 97%), hydrochloric acid (HCl, 37%), graphene oxide (paste, nonexfoliated), L-arginine (reagent grade, ≥98%), guanidine acetic acid (99%), L-proline (≥99%), L-aspartic acid (reagent

https://doi.org/10.1021/acs.iecr.3c02400
Ind. Eng. Chem. Res. 2023, 62, 15202−15211

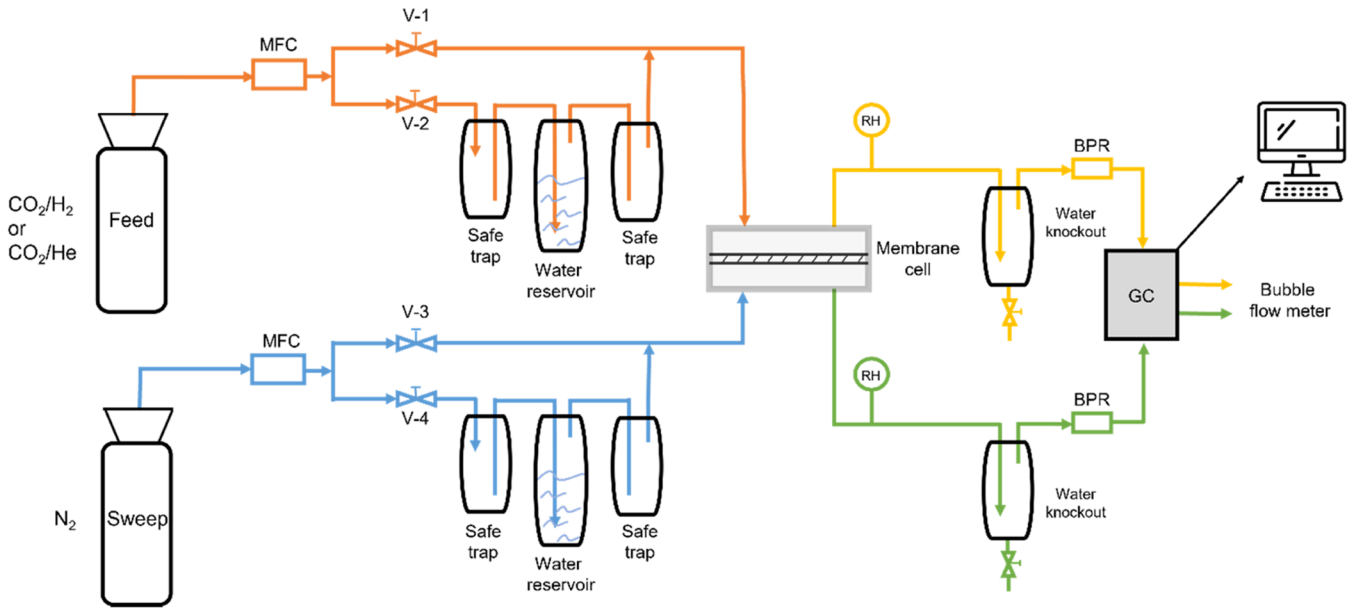

Figure 2. Scheme of a humid mixed gas permeation testing rig for CO_2/H_2 and CO_2/He separation. MFC: mass flow controller, RH: relative humidity sensor, BPR: back pressure regulator, and GC: gas chromatography.

grade, ≥98%), and potassium hydroxide (anhydrous, ≥99.95% trace metals basis) were purchased from Sigma-Aldrich, Norway. Acetone (≥98%), ethanol absolute (EtOH), and glycine (≥99.95%) were purchased from VWR, Norway. Polysulfone (PSF) ultrafiltration (UF) membranes (GR40PP) were purchased from Alfa Laval Nordic AS, Denmark, with a molecular weight cutoff (MWCO) of 20k. The epoxy glue Loctite 3430 was purchased from TOOLS, Norway, and the Avery Dennison 180 aluminum foils used to seal the membranes were received from Norsk Filmtrykk AS, Norway. The CO_2/He gas mixture (10 vol % CO_2 in He) used for the permeation test was received from Linde Gas AS, Norway.

2.2. Synthesis of PVAm/(PVA-GO). Optimized synthesis procedures from our prior work, including PVAm purification, preparation of GO solutions, synthesis of PVA-GO solutions, and preparation of PVAm/(PVA-GO) solutions, were applied to ensure a homogeneous membrane matrix and good gas separation performance, part of which can be found in the literature.[17,21,22] For the readers' convenience, a brief description is given as follows: (1) PVAm purification: Lupamin 9095 was precipitated using an acetone/EtOH mixture, then the precipitation was filtrated, washed, and dried, and it was repeated several times in order to obtain purified PVAm; after that, a certain amount of the PVAm solution was prepared with the adjusted pH value as 10 using 5 M NaOH. (2) The GO nanosheets were dissolved in DI water to prepare a 1 mg/g GO solution. Next, 5 M NaOH was added to adjust the pH to 10. Then, the dispersed solution was sonicated again in ultrasonic disintegration (Vibra-Cell Ultrasonic Liquid Processor) at an amplitude of 60% in an ice bath, with a three-second pulse, two-second break, and 6 h of operation time to ensure exfoliation and a thorough dispersion. (3) A certain amount of the GO dispersion was dropwise added to the 7 wt % PVA solution, which was prepared by adding 7 g of PVA in 93 mL of DI water at 95 °C with refluxing until dissolving completely. The solution was then vigorously stirred under 60 °C to obtain a very fine brown-to-black PVA-GO solution with relatively high viscosity containing 0.034 wt % GO and 0.046 wt % PVA. (4) A certain amount of PVA-GO and PVAm was mixed to obtain a 1.5 wt % PVAm/(PVA-GO) solution.

2.3. Preparation of the Membrane and the Membrane Module. All guanidine-based and amino acid-based salts used in this work were synthesized by mixing a stoichiometric number of mobile carriers with KOH in DI to prepare a 5 wt % salt solution. A certain amount (10, 20, 30, and 40 wt %) of four different salts and PVAm/(PVA-GO) was mixed into the solutions. The total solid concentration was diluted to 1.5 wt % in DI water. The salt content (ω_{salt}, wt %) in all of the membranes was calculated by eq 1

$$\omega_{salt} = \frac{m_{salt}}{m_{salt} + m_{PVAm/(PVA\text{-}GO)}} \times 100\% \quad (1)$$

where $m_{PVAm/(PVA\text{-}GO)}$ is the weight of PVAm/(PVA-GO) and m_{salt} is the weight of salts as mobile carriers.

All membranes were coated by dip-coating using the dip-coating machine (KCV NIMA, Biolin Scientific, Finland) under identical conditions (coating speed: 149.96 mm/min). First, commercially available PSF UF membranes as support membranes were washed with warm tap water for 1 h (~45 °C) and later with DI water for at least half an hour. Then, the mounted membranes were coated by dip-coating with the membrane solution, and the membranes were soaked in the membrane solution for 30 s. Afterward, the membranes were dried in air for approximately 8 h. After that, the coated membranes were turned upside-down for the second coating, following the same procedure. Before testing, membranes were treated at 90 °C in a ventilated oven for 1 h in order to induce physical cross-linking.

2.4. Characterization of Materials and Membranes. A Fourier transform infrared (FTIR) spectrometer (Thermo Nicolet Nexus) was used with a smart endurance reflection cell (Golden Gate high-performance single reflection monolithic diamond ATR) to study the chemical bonds of the dry samples. FTIR spectra of PVAm/(PVA-GO), four different guanidine-based and amino acid-based salts, and PVAm/(PVA-GO) with four different salts (ArgK, GuaK, ProK, and

https://doi.org/10.1021/acs.iecr.3c02400
Ind. Eng. Chem. Res. 2023, 62, 15202−15211

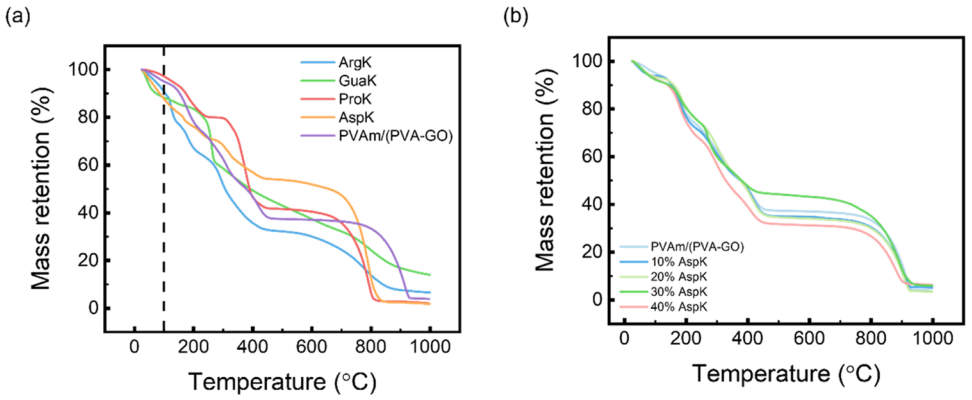

Figure 3. TGA results of (a) guanidine-based salts ArgK and GuaK, amino acid-based salts ProK and AspK, PVAm/(PVA-GO), and (b) PVAm/(PVA-GO)/AspK nanocomposites with different contents of AspK.

AspK) under different ratios were measured within the scan range between 750 and 4000 cm^{-1}. It needs to be mentioned that in this work, all of the dry samples of materials were dried at 40 °C under a 220 mbar vacuum overnight to avoid the crystallization of PVAm.

Thermogravimetric analysis (TGA, Thermal Scientific Q500) was used to analyze the thermal stability of samples. The TGA experiments were performed in a N_2 atmosphere. Overall, 5−10 mg of samples was placed in the sample holder, and all of the samples were heated with the same preset heating protocol, and the heating rate was set at 5 °C/min. N_2 was used as the purge and cooling gas with a flow rate of 20 mL/min. The surface and cross-sectional morphologies of the membranes were obtained using a field emission scanning microscope (FE-SEM, ZEISS Supra-55 VP, manufactured by Carl Zeiss NTS GmbH, Germany). The membrane samples were cryogenically fractured in liquid nitrogen to get clear cross-sectional figures, and all membrane samples were coated with a thin layer of gold with a sputter coater to enhance electrical conductivity in order to get clearer figures to analyze.

The mixed gas separation performance of the prepared membranes was tested using a homemade apparatus (Figure 2). More details can be found in ref 23.

The gas mixture of CO_2/He or CO_2/H_2 (10 vol % CO_2 in the binary mixtures) was used as the feed gas under 1.7 bar, and N_2 was used as the sweep gas at the permeate side for the lab-scale testing (at approximately 1.05 bar) instead of applying vacuum pressures. All of the optimization tests were performed at 25 °C and kept under full humidity in both feed gas and sweep gas streams. After that, the optimized membrane was tested with CO_2/H_2 (10 vol % CO_2/90 vol % H_2) under different temperature conditions from 25 to 65 °C with other conditions kept the same as the CO_2/He tests. The concentrations of CO_2 and He or H_2 from the sweep side were measured with a calibrated gas chromatograph (490 Micro GC, Agilent).

The permeance ($\frac{P_i}{l}$, GPU) of component "i" can be obtained by eq 2

$$\frac{P_i}{l} = \frac{N_{perm}(1 - y_{H_2O})y_i}{A(p_{i,feed} - p_{i,perm})} \quad (2)$$

where P_i is the permeability of component "i" expressed in the unit of Barrer and N_{perm} is the total permeate flow rate measured using a bubble flow meter on the permeate side, as shown in Figure 2, y_{H_2O} is the mole fraction of water in the permeate flow calculated according to the relative humidity and the vapor pressure based on the testing condition, y_i is the molar fraction gas component "i" on the permeate side, A is the effective membrane area, and $p_{i,feed}$ and $p_{i,perm}$ are the partial pressures of gas component "i" in the feed and permeate side, respectively.

The gas selectivity (separation factor) can be determined by eq 3, described using ratios of mole fractions between two gas components "i" and "j":

$$\alpha_{i/j} = \frac{y_i/y_j}{x_i/x_j} \quad (3)$$

where y_i and y_j are the mole fractions of gas components "i" and "j" on the permeate side and x_i and x_j are the mole fractions of gas components "i" and "j" on the feed side.

Due to strict safety requirements in our laboratory, the CO_2/He gas mixture was used instead of CO_2/H_2 during the membrane material optimization. After the optimized membrane material was determined, the membranes were measured with a CO_2/H_2 gas mixture to test the CO_2/H_2 gas separation performance. Helium was used to represent hydrogen because it has the closest molecular size to H_2,[24] and, according to our previous work, H_2 permeance showed very similar data to the helium permeance in CO_2/He mixture and CO_2/H_2 mixture testing, with only ~6% deviation, lower than the accepted deviation (10%) in this work.[22]

Four different mobile carriers were added separately to PVAm/(PVA-GO) membranes (PSF UF membranes as porous support), and their effects on the CO_2/He separation performance were compared to select the optimal salts and ratio between PVAm/(PVA-GO) and the salts. At least three membranes with different loadings of each salt were tested to ensure the stability of the membrane performance and reproducibility. The average values from the tests were used for each reported data point in this work.

3. RESULTS AND DISCUSSION

3.1. Thermal Properties. TGA was used to evaluate the thermal stabilities of all of the membrane materials, and the results are shown in Figures 3 and S1.

As shown in Figure 3a, initially, weight losses of all samples due to the water loss at the temperature range (≤100 °C) are observed, and the weight changes are different for different salts, reflecting their different water uptake capacities in the air.

https://doi.org/10.1021/acs.iecr.3c02400
Ind. Eng. Chem. Res. 2023, 62, 15202−15211

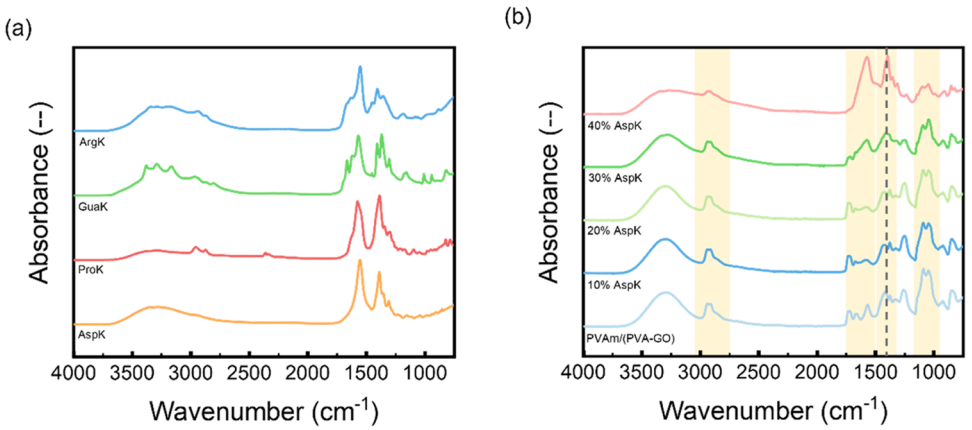

Figure 4. FTIR spectra of (a) ArgK, GuaK, ProK, and AspK, and (b) PVAm/(PVA-GO)/AspK nanocomposites with different contents of AspK.

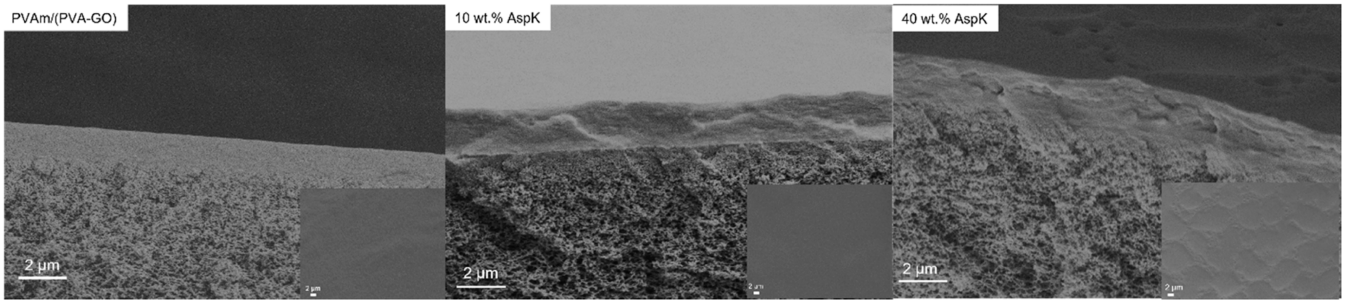

Figure 5. Cross-sectional and surface FESEM images (insets) of the neat PVAm/(PVA-GO) membrane and PVAm/(PVA-GO) membranes containing 10 and 40 wt % AspK.

For instance, AspK has decreased its weight to 87 wt % (the most decreased) since AspK has higher water uptake ability than other salts in this work, while ProK shows the lowest weight (water) loss. It also shows that, in general, the two guanidine-based salts also have high water sorption capacity. At high temperatures (above 800 °C) after the decomposition occurs, the weight is from the remaining carbon since N_2 was used as the purge and cooling gas in the system. Even though the carbon-based main chain and groups of ArgK are more than those of GuaK, GuaK shows the highest residual mass, which may be because the primary amino group and guanidine groups in these salts have a higher possibility of forming cross-linked structures.[25] The two amino acid salts show similar residual mass.

The TGA curves of PVAm/(PVA-GO)/AspK nanocomposite membranes with four different AspK contents are presented in Figure 3b. By incorporating AspK into the PVAm/(PVA-GO) matrix, the weight loss under ≤100 °C, i.e., the water loss, increases. Samples containing different salts show similar trends, as shown in Figure S1, so it seems that adding both guanidine-based salts and amino acid salts increases the water sorption capacity of the materials. Moreover, by increasing the salt content to 30 or 40 wt %, the decomposition stage becomes slightly different from the samples of lower salt contents, most likely due to the fact that phase separation starts in the materials over a certain salt loading and that the interfacial interactions between PVAm/(PVA-GO) and salts become more difficult.

3.2. Chemical Structure Analysis. FTIR analysis was employed to investigate the interactions between PVAm/(PVA-GO) and the guanidine-based or amino acid-based salts (Figure 4).

As seen from Figure 4a, a broad peak can be observed for all samples in the relatively high energy region (approximately from 3500 to 3000 cm^{-1}), which is associated with NH_3^+ stretching vibrations.[16] In the energy range of 1750− 1400 cm^{-1}, two clear peaks can be noted, which can be assigned to the $-COO^-$ (in the carboxyl group) asymmetric stretching vibration and symmetric stretching vibration.[26] Considering ArgK, two small but clear characteristic peaks can be found at approximately 1650 cm^{-1} and approximately 1400 cm^{-1}, which correspond to the guanidino group and C−C−N asymmetric bonding.[27] Similar characteristic peaks can also be found for GuaK since the chemical structures of ArgK and GuaK are similar. For ProK, two characteristic peaks can be observed at approximately 1490 and 1300 cm^{-1}, corresponding to the C−H asymmetric stretching of $-CH_2$.[28] Moreover, in AspK, a small peak can be observed at approximately 1400 cm^{-1}, which can be assigned to the $-COO^-$ symmetric stretching as discussed above.[29] Peaks in the lower wavenumber are mainly due to C−H or C−C stretching and are thus not included in the discussion.

A comparison of the FTIR spectra of PVAm/(PVA-GO) and PVAm/(PVA-GO)/AspK of various AspK loadings is displayed in Figure 4b. Some characteristic peaks of AspK can be observed in the nanocomposites. With increasing AspK content, the characteristic peaks of AspK become clearer. Furthermore, there is a peak shift, approving that interfacial interaction happens between PVAm/(PVA-GO) and AspK, such as the hydrogen bonding between −OH groups in PVAm/(PVA-GO) (membrane matrix) and amine groups in AspK.[30] The FTIR spectra of other PVAm/(PVA-GO) and salt composites containing ProK, GuaK, and ArgK are given in

https://doi.org/10.1021/acs.iecr.3c02400
Ind. Eng. Chem. Res. 2023, 62, 15202−15211

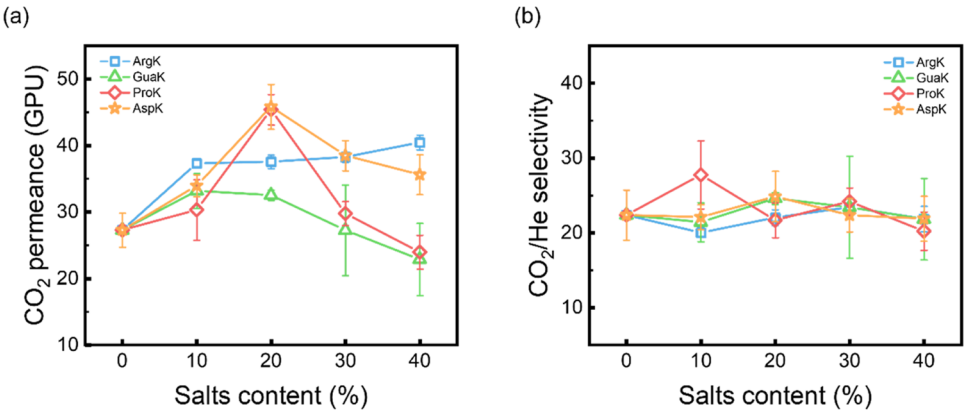

Figure 6. CO_2/He gas separation performance of PVAm/(PVA-GO) and PVAm/(PVA-GO)/salts with four different ratios: (a) CO_2 permeance and (b) CO_2/He selectivity; tested under a feed pressure of 1.7 bar and approximately 100% relative humidity.

Figure S2, which show similar patterns as that of PVAm/(PVA-GO)/AspK.

3.3. Membrane Morphology. The membrane surface morphology and selective layer cross sections have been investigated using FESEM. Figure 5 presents the SEM images of neat PVAm/(PVA-GO) membranes and two different AspK atoms in the PVAm/(PVA-GO) membrane matrix.

FESEM images in Figure 5 show that a layer with a thickness of ~1.8 μm was successfully coated on the PSF UF flat sheet substrate. As shown in the figure, the influence of increasing AspK content in the membrane on the selective layer thickness is negligible. Due to the same procedure of coating solution preparation and coating, the selective layer thicknesses of the membrane matrices with different salts and different contents are similar.

In addition, Figure 5 shows that both the neat PVAm/(PVA-GO) membrane and membranes containing 10 wt % Asp present a defect-free surface with no obvious pore filling in the substrates. However, the membrane of 40 wt % AspK presents an uneven surface, which is believed to be because of the unwanted salt-induced phase separation in the membrane matrix. Surface SEM images for the PVAm/(PVA-GO) membrane with 40 wt % of other salts are shown in Figure S3. Further, 40 wt % ArgK shows an even membrane surface, different from the work reported by Dai et al.[16] It can be explained by some shifted peaks in the FTIR spectra, as shown in Figure S2c, which is strong evidence of interfacial interactions, including hydrogen bonding between the PVAm/(PVA-GO) membrane matrix and the salts. The membrane surface morphologies of membranes containing 40 wt % ProK and 40 wt % GuaK seem similar to that of 40 wt % AspK, also due to the phase separation or poor compatibility between the PVAm/(PVA-GO) matrix with the added salts at high loading.

3.4. Mixed Gas Separation Study. *3.4.1. Effect of Mobile Carrier Types and Loading.* In a CO_2-selective facilitated transport membrane, CO_2 transports across the membrane matrix through a reversible reactive pathway in addition to the solution-diffusion transport,[31] often with the presence of water, leading to relatively high CO_2/He gas separation performance. Adding mobile carriers is expected to introduce positive effects to CO_2-facilitated transport, resulting in higher CO_2 permeance, selectivity, or even both.

The effects of mobile carriers are studied by adding the four selected salts (ArgK, GuaK, ProK, and AspK) into the PVAm/PVA-GO membrane as mobile carriers. The CO_2/He separation performances of the PVAm/(PVA-GO) membrane and PVAm/(PVA-GO) membranes containing different mobile carriers with various contents are presented in Figure 6.

As shown in Figure 6, the separation performance of neat PVAm/(PVA-GO) membranes has already reached the CO_2/He selectivity of as high as 22 and CO_2 permeance of 27.2 GPU due to the facilitated transport effect of PVAm and the "barrier effect" of PVA-GO.[22]

The effects of mobile carriers on the CO_2 permeance are shown in Figure 6a. Adding selected mobile carriers resulted in a significant increase in CO_2 permeance, but the effects of the loadings are different depending on the types of salts. At a relatively low loading of 10%, adding ArgK resulted in the highest increase in CO_2 permeance from 27.2 GPU to 37.3, an approximately 37% increase. However, increasing ArgK loading to up to 40 wt % does not further improve its CO_2 permeance; the CO_2 permeance remains nearly the same, or the differences are within the error range. It may be due to the poor compatibility between ArgK and the membrane matrix at a high loading. A similar result was observed in the case of GuaK. Adding 10 wt % GuaK into the membrane matrix, the CO_2 permeance slightly increases. However, upon further increase of the GuaK loading, the CO_2 permeance dramatically decreases. It was also observed that the solution at a high loading became unstable and caused salt precipitation in the two GuaK-based membrane solutions on the third day. Thus, a higher loading of two guanidine-based salts, ArgK and GuaK, may have led to unstable membrane interfacial interaction and phase separation, as shown in Figure S3, exhibiting negative effects on the CO_2/He gas separation performance. In addition, as mobile carriers, the more bulky guanidine-based salts may present lower mobility in the membrane matrix and less accessible amine groups for the facilitated transport of CO_2.

According to the testing results, the optimal CO_2 permeances are presented by the amino acid-based membranes containing ProK or AspK at the 20 wt % loading; the CO_2 permeance of ~46 GPU is achieved, 67% increase compared to the neat PVAm/(PVA-GO) nanocomposite membrane. Further increasing the loadings, both membranes' CO_2 permeances start to drop. This trend, CO_2 permeance first increasing and then decreasing, may be explained by their positive effects by the mobile carriers' CO_2-philicity at the relatively low loading range (10−20 wt % ProK or AspK).

https://doi.org/10.1021/acs.iecr.3c02400
Ind. Eng. Chem. Res. 2023, 62, 15202−15211

With an increasing loading, more CO_2-philic groups are introduced into the membrane matrix, which are also hydrophilic groups, leading to a higher water swelling degree of the membrane and hence higher gas diffusion and mobile carrier mobility and, consequently, significantly increased CO_2 permeance. However, when salt loadings are over a certain limit, i.e., ≥30 wt %, the salt dispersion inside the membrane matrix becomes more difficult, and phase separation occurs. The presence of more salts causes worse stability and more phase separation in the membrane matrix; thus, the active mobile carriers in the membrane matrix become less accessible, and the CO_2 permeance decreases.

On the other hand, a higher degree of water swelling in CO_2-selective facilitated transport membranes implies a better CO_2 facilitated transport effect according to the strong water involvement in the reversible reaction between CO_2 and amino groups. Thus, adding highly hydrophilic amino acid salts, giving higher water capacity to the membranes, led to better CO_2 separation performance than that of guanidine-based salts. Moreover, compared with ProK, AspK has a higher mobility in the membrane matrix due to its more loose and linear structure, which also benefits CO_2 transport and results in high CO_2 permeation performance (with 20 wt % loading).[32] Since further increasing AspK loading led to a decrease in CO_2 permeance, the optimal membrane to achieve the highest CO_2 permeance is an AspK-based membrane at a 20% loading, with which the CO_2/He selectivity was kept nearly the same as the pristine PVAm/PVA-GO membrane (Figure 6b).

Figure 6b presents the effects of mobile carriers and loadings on the CO_2/He selectivity. As seen in the plots, the CO_2/He selectivity does not exhibit a significant change in the membranes containing different salts with different loadings, showing selectivity similar to that of the pristine PVAm/(PVA-GO) nanocomposite membranes; the deviations of the data are in the error range (standard deviation). Similar trends were reported by other researchers.[16,17,33] One exception is the ProK-based membrane at a 10% loading, in which the CO_2/He selectivity increased from 22 to 28, showing a 27% increase, and the CO_2 permeance is also slightly increased. The ProK-based membrane showing better CO_2/He selectivity than that of AspK may be attributed to the higher reaction rate constant of proline (10.64 in the amine group) than that of aspartic acid (9.9 in the amine group or 3.9 in side chains).[20,34] High CO_2/He or CO_2/H_2 selectivity is beneficial to achieve high-purity products.[35] Thus, ProK-based membranes can potentially be a promising solution for industrial applications when high CO_2 purification is desired.

To sum up, the AspK-based membrane at a 20 wt % AspK loading is determined to be the optimal membrane for the most improved CO_2 permeance. If a higher selectivity is more critical, ProK at a 10% loading in PVAm/(PVA-GO) should be considered.

3.4.2. Effect of Temperature. As a key characteristic of facilitated transport membranes, the operating temperature substantially influences membrane separation performances, as explained by the complex transport mechanism in the membrane matrix, including reversible reaction kinetics of facilitated transport membranes and diffusion of the CO_2-carrier complex.[36]

The optimized PVAm/(PVA-GO) nanocomposite membrane with a 20 wt % AspK loading was fabricated and tested to evaluate its CO_2/H_2 separation performance. The testing conditions are the same as used in the membrane optimization stage, at a feed pressure of 1.7 bar and ∼100% relative humidity and different temperatures from 25 to 65 °C, but the gas mixture is changed from CO_2/He to CO_2/H_2.

The temperature dependences of the CO_2/H_2 separation performance were investigated. The CO_2 and H_2 permeance results are presented in Figure 7. As expected, both the CO_2 and H_2 permeance increase with increasing temperature; the maximum CO_2 permeance value of 62.4 GPU is reached at 65 °C, while the H_2 permeance is 6.2 GPU. CO_2 permeance with temperature can be explained by the accelerated reversible reaction kinetics and the higher mobility of the CO_2−amine complex with increasing temperature. Furthermore, this trend follows the Arrhenius law described in eq 4.[37]

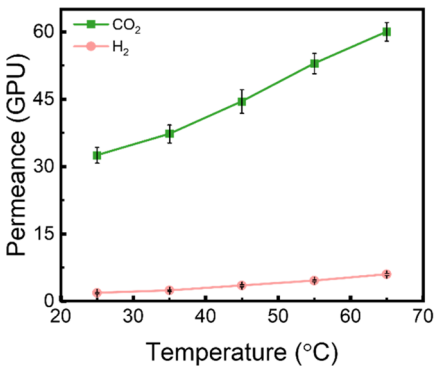

Figure 7. Effect of testing temperature on PVAm/(PVA-GO) with 20 wt % AspK nanocomposite membranes on CO_2 and H_2 permeance for CO_2/H_2 separation performance.

$$\frac{P_i}{l} = P_0 \exp\left(-\frac{E_a}{RT}\right) \tag{4}$$

where P_0 is a pre-exponential factor, E_a is the gas activation energy of permeation, R is the gas constant (8.314×10^{-3} kJ/(mol K)), and T is the temperature (K). When the selective layer was fully humidified, the E_a for CO_2 was 13.1 kJ/mol and that for H_2 was 25.5 kJ/mol. The higher activation energy for permeation of H_2 is attributed to the lower H_2 solubility and the lack of reactive pathways in the membrane matrix. The relatively higher E_a value of H_2 explains the trend that the H_2 permeance increased faster than that of CO_2 with increasing temperature, resulting in decreasing CO_2/H_2 selectivity. This tendency is similar to a previous report by Han et al.[38]

As a comparison, the overall CO_2/H_2 gas separation performance of the optimized PVAm/(PVA-GO) membranes containing 20 wt % AspK and that of 10 wt % ProK were tested using the CO_2/H_2 mixture and the experimental data were plotted against the CO_2/H_2 upper bound,[10,39] as presented in Figure 8. The developed mobile-carrier-enhanced membranes in this work exhibit CO_2/H_2 separation performance far over the upper bound. The PVAm/(PVA-GO) with 20 wt % AspK with a 1.8 μm selective layer thickness shows the highest CO_2 permeability of 112.3 Barrer under 65 °C, which is among the best-performed CO_2 permeability of membranes under mild separation conditions for CO_2/H_2 separation, as reported in the literature; higher gas separation performances were reported under elevated testing temperatures of ≥100 °C.[40] The 10 wt % ProK-based membrane exhibited the highest CO_2/H_2 selectivity of 24 with the CO_2 permeability of 36.7 Barrer under 25 °C. It has to be

https://doi.org/10.1021/acs.iecr.3c02400
Ind. Eng. Chem. Res. 2023, 62, 15202−15211

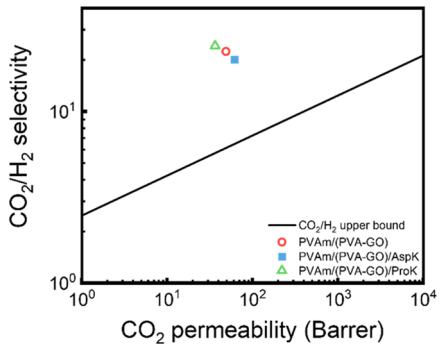

Figure 8. CO_2/H_2 gas separation performance of neat PVAm/(PVA-GO) and PVAm/(PVA-GO) contaning 20 wt % AspK (blue cube) and PVAm/(PVA-GO) containing 10 wt % ProK (green triangle) in comparison with the CO_2/H_2 upper bound.

mentioned that the CO_2 permeability data for this work were calculated using the thickness of the selective layer from FE-SEM images, as discussed above, by ignoring the resistance in the porous support. Thus, the actual permeability for the material of the selective layer should be higher than the data presented in this work.

4. CONCLUSIONS

Facilitated transport membranes with a PVAm/(PVA-GO) based nanocomposite selective layer containing four selected mobile carriers (two guanidine-based salts and two amino acid salts) were fabricated and tested for the CO_2/H_2 separation. The effects of adding mobile carriers were investigated by studying the effects of their loadings on the CO_2/H_2 separation performances. The presence of the selected salts benefits CO_2-facilitated transport and increases the CO_2 permeance without sacrificing CO_2/H_2 selectivity or vice versa. Adding the two amino acid salts leads to higher CO_2 permeance, most likely due to their higher carrier mobility than adding guanidine salts. The gas separation performance is found to be temperature-dependent. Increasing the temperature promotes CO_2 transport, leading to improved CO_2 permeability. By adding 20 wt % AspK as a mobile carrier in the PVAm/(PVA-GO) matrix, the CO_2 permeance increased to a maximum of 62.4 GPU under 65 °C, and under 25 °C, the CO_2 permeance also increased to 34.4 GPU with a nearly constant CO_2/H_2 selectivity of 22. These data are far above the upper bound and among the best-performed membranes in the literature under similar testing conditions. Moreover, the addition of 10 wt % ProK in the membrane matrix increased the CO_2/H_2 selectivity by ≥25%.

This study followed the general rules of picking mobile carriers, including the selected molecules should be basic, can have a reversible reaction with CO_2, and the molecules should have a suitable size to ensure mobility while being kept in the membrane matrix. In this work, we found that mobile carriers with a more relaxed structure may bring in better gas separation performance, a higher CO_2-mobile carriers reaction rate leads to higher CO_2 selectivity, and mobile carriers with higher hydrophilicity exhibit a more positive effect of CO_2 separation performance. Moreover, the selected mobile carrier molecules should be soluble and stable in the membrane casting solutions.

■ ASSOCIATED CONTENT

Supporting Information

The Supporting Information is available free of charge at https://pubs.acs.org/doi/10.1021/acs.iecr.3c02400.

Thermogravimetric analysis; Fourier transform infrared; and membrane surface morphology of PVAm/(PVA-GO)/ArgK, PVAm/(PVA-GO)/ProK, and PVAm/(PVA-GO)/GuaK nanocomposite membranes (PDF)

■ AUTHOR INFORMATION

Corresponding Author

Liyuan Deng − *Department of Chemical Engineering, Norwegian University of Science and Technology (NTNU), Trondheim NO-7491, Norway;* orcid.org/0000-0003-4785-4620; Phone: +47 73594112; Email: liyuan.deng@ntnu.no

Authors

Wenqi Xu − *Department of Chemical Engineering, Norwegian University of Science and Technology (NTNU), Trondheim NO-7491, Norway*

Arne Lindbråthen − *Department of Chemical Engineering, Norwegian University of Science and Technology (NTNU), Trondheim NO-7491, Norway*

Xueru Wang − *Department of Chemical Engineering, Norwegian University of Science and Technology (NTNU), Trondheim NO-7491, Norway; Laboratory for Multiscale Mechanics and Medical Science, SV Lab, School of Aerospace, Xi'an Jiaotong University, Xi'an 710049, China*

Zhongde Dai − *School of Carbon Neutrality Future Technology, Sichuan University, Chengdu 610065, China;* orcid.org/0000-0002-3558-5403

Complete contact information is available at: https://pubs.acs.org/10.1021/acs.iecr.3c02400

Author Contributions

W.X. contributed to methodology, formal analysis, validation, investigation, writing—original draft, and visualization. A.L., X.W., and Z.D. contributed to writing—review and editing. L.D. contributed to conceptualization, writing—review and editing, supervision, project administration, and funding acquisition. All authors have read and agreed to the published version of the manuscript.

Notes

The authors declare no competing financial interest.

■ ACKNOWLEDGMENTS

This work is a part of the FaT H2 project supported by the Research Council of Norway (No. 294533).

■ REFERENCES

(1) Cartwright, E. D. *Code Red"—Recent IPCC Report Warns Time is Running Out on Climate Change*, 2021; Vol. 3.

(2) Hong, W. Y. A techno-economic review on carbon capture, utilisation and storage systems for achieving a net-zero CO2 emissions future. *Carbon Capture Sci. Technol.* **2022**, 3, No. 100044.

(3) Prestipino, M.; Piccolo, A.; Polito, M. F.; Galvagno, A. Combined Bio-Hydrogen, Heat, and Power Production Based on Residual Biomass Gasification: Energy, Exergy, and Renewability Assessment of an Alternative Process Configuration. *Energies* **2022**, *15* (15), 5524. ARTN 5524

(4) Sarangi, P. K.; Nanda, S. Biohydrogen Production Through Dark Fermentation. *Chem. Eng. Technol.* **2020**, *43* (4), 601−612.

(5) Nnabuife, S. G.; Ugbeh-Johnson, J.; Okeke, N. E.; Ogbonnaya, C. Present and Projected Developments in Hydrogen Production: A Technological Review. *Carbon Capture Sci. Technol.* **2022**, *3*, No. 100042.
(6) (a) Ansaloni, L.; Deng, L. Advances in Polymer-Inorganic Hybrids as Membrane Materials. In *Recent Developments in Polymer Macro, Micro and Nano Blends*; Visakh, P. M.; Markovic, G.; Pasquini, D., Eds.; Elsevier, 2017; Chapter 7, 2017; pp 163−206. (b) Buckingham, J.; Reina, T. R.; Duyar, M. S. Recent advances in carbon dioxide capture for process intensification. *Carbon Capture Sci. Technol.* **2022**, *2*, No. 100031. (c) Dai, Z.; Ansaloni, L.; Deng, L. Recent advances in multi-layer composite polymeric membranes for CO2 separation: A review. *Green Energy Environ.* **2016**, *1* (2), 102−128. (d) Hägg, M.-B.; Deng, L. Membranes in gas separation. In *Handbook of Membrane Separations: Chemical, Pharmaceutical, Food, and Biotechnological Applications*, 2nd ed.; CRC Press, 2015; pp 143−180.
(7) (a) Sazali, N.; Mohamed, M. A.; Salleh, W. N. W. Membranes for hydrogen separation: a significant review. *Int. J. Adv. Manuf. Technol.* **2020**, *107* (3−4), 1859−1881. (b) Pal, N.; Agarwal, M.; Maheshwari, K.; Solanki, Y. S. A review on types, fabrication and support material of hydrogen separation membrane. *Mater. Today-Proc.* **2020**, *28*, 1386−1391. (c) Salleh, W.; Ismail, A. F. Carbon membranes for gas separation processes: Recent progress and future perspective. *J. Membr. Sci. Res.* **2015**, *1* (1), 2−15.
(8) Pal, N.; Agarwal, M. Advances in materials process and separation mechanism of the membrane towards hydrogen separation. *Int. J. Hydrogen Energy* **2021**, *46* (53), 27062−27087.
(9) Galizia, M.; Chi, W. S.; Smith, Z. P.; Merkel, T. C.; Baker, R. W.; Freeman, B. D. 50th Anniversary Perspective: Polymers and Mixed Matrix Membranes for Gas and Vapor Separation: A Review and Prospective Opportunities. *Macromolecules* **2017**, *50* (20), 7809−7843.
(10) Robeson, L. M. The upper bound revisited. *J. Membr. Sci.* **2008**, *320* (1−2), 390−400.
(11) Freeman, B. D. Basis of permeability/selectivity tradeoff relations in polymeric gas separation membranes. *Macromolecules* **1999**, *32* (2), 375−380.
(12) Rafiq, S.; Deng, L.; Hägg, M.-B. Role of Facilitated Transport Membranes and Composite Membranes for Efficient CO2 Capture − A Review. *ChemBioEng Rev.* **2016**, *3* (2), 68−85.
(13) Saeed, M.; Rafiq, S.; Bergersen, L. H.; Deng, L. Tailoring of water swollen PVA membrane for hosting carriers in CO2 facilitated transport membranes. *Sep. Purif. Technol.* **2017**, *179*, 550−560. (13a) Deng, L.; Hägg, M.-B. Swelling behavior and gas permeation performance of PVAm/PVA blend FSC membrane. *J. Membr. Sci.* **2010**, *363* (1), 295−301.
(14) Pelton, R. Polyvinylamine: a tool for engineering interfaces. *Langmuir* **2014**, *30* (51), 15373−15382. From NLM PubMed-not-MEDLINE.
(15) Xu, W. Membrane process design for biohydrogen purification with simultaneous CO2 capture: feasibility and techno-economic assessment. *submitted to Chemical Engineering Science* 2023.
(16) Dai, Z. D.; Deng, J.; Ansaloni, L.; Janakiram, S.; Deng, L. Y. Thin-film-composite hollow fiber membranes containing amino acid salts as mobile carriers for CO2 separation. *J. Membr. Sci.* **2019**, *578*, 61−68.
(17) Janakiram, S.; Espejo, J. L. M.; Hoisaeter, K. K.; Lindbrathen, A.; Ansaloni, L.; Deng, L. Y. Three-phase hybrid facilitated transport hollow fiber membranes for enhanced CO2 separation. *Appl. Mater. Today* **2020**, *21*, No. 100801.
(18) Zhao, Y.; Ho, W. W. CO2-selective membranes containing sterically hindered amines for CO2/H2 separation. *Ind. Eng. Chem. Res.* **2013**, *52* (26), 8774−8782. (18a) Zou, J.; Ho, W. S. W. CO2-selective polymeric membranes containing amines in crosslinked poly(vinyl alcohol). *J. Membr. Sci.* **2006**, *286* (1−2), 310−321.
(19) Zhang, S.; He, L. N. Capture and Fixation of CO2 Promoted by Guanidine Derivatives. *Aust. J. Chem.* **2014**, *67* (7), 980−988. (19a) Raczy?ska, E. D.; Cyrański, M. K.; Gutowski, M.; Rak, J.; Gal, J. F.; Maria, P. C.; Darowska, M.; Duczmal, K. Consequences of proton transfer in guanidine. *J. Phys. Org. Chem.* **2003**, *16* (2), 91−106. (19b) Custelcean, R.; Garrabrant, K. A.; Agullo, P.; Williams, N. J. Direct air capture of CO2 with aqueous peptides and crystalline guanidines. *Cell Rep. Phys. Sci.* **2021**, *2* (4), No. 100385. ARTN 100385
(20) Zhang, Z. E.; Rao, S.; Han, Y.; Pang, R. Z.; Ho, W. S. W. CO2-selective membranes containing amino acid salts for CO2/ N2 separation. *J. Membr. Sci.* **2021**, *638*, No. 119696. ARTN 119696
(21) Kim, T. J.; Vralstad, H.; Sandru, M.; Hagg, M. B. Separation performance of PVAm composite membrane for CO2 capture at various pH levels. *J. Membr. Sci.* **2013**, *428*, 218−224. (21a) Kashyap, S.; Pratihar, S. K.; Behera, S. K. Strong and ductile graphene oxide reinforced PVA nanocomposites. *J. Alloys Compd.* **2016**, *684*, 254−260.
(22) Xu, W. Q.; Lindbrathen, A.; Janakiram, S.; Ansaloni, L.; Deng, L. Y. Enhanced CO2/H2 separation by GO and PVA-GO embedded PVAm nanocomposite membranes. *J. Membr. Sci.* **2023**, *671*, No. 121397. ARTN 121397
(23) Dai, Z.; Deng, J.; Yu, Q.; Helberg, R. M. L.; Janakiram, S.; Ansaloni, L.; Deng, L. Fabrication and Evaluation of Bio-Based Nanocomposite TFC Hollow Fiber Membranes for Enhanced CO2 Capture. *ACS Appl. Mater. Interfaces* **2019**, *11* (11), 10874−10882.
(24) Dai, Z. D.; Ansaloni, L.; Deng, L. Y. Precombustion CO2 Capture in Polymeric Hollow Fiber Membrane Contactors Using Ionic Liquids: Porous Membrane versus Nonporous Composite Membrane. *Ind. Eng. Chem. Res.* **2016**, *55* (20), 5983−5992.
(25) Fraenkel-Conrat, H.; Olcott, H. S. The reaction of formaldehyde with proteins. V. Cross-linking between amino and primary amide or guanidyl groups. *J. Am. Chem. Soc.* **1948**, *70* (8), 2673−2684. (25a) Friedman, M. Crosslinking amino acids–stereochemistry and nomenclature. *Adv. Exp. Med. Biol.* **1977**, *86B*, 1−27. From NLM Medline.
(26) Richner, G.; Puxty, G. Assessing the Chemical Speciation during CO2 Absorption by Aqueous Amines Using in Situ FTIR. *Ind. Eng. Chem. Res.* **2012**, *51* (44), 14317−14324.
(27) Shriner, R. L.; Hermann, C. K.; Morrill, T. C.; Curtin, D. Y.; Fuson, R. C. *The Systematic Identification of Organic Compounds*; John Wiley & Sons, 2003. Liu, W. G.; Zhang, J. R.; Cao, Z. Q.; Xu, F. Y.; Yao, K. D. A chitosan-arginine conjugate as a novel anticoagulation biomaterial. *J. Mater. Sci.: Mater. Med.* **2004**, *15* (11), 1199−1203.
(28) Bhuvaneswari, R.; Karthikeyan, S.; Selvasekarapandian, S.; Pandi, D. V.; Vijaya, N.; Araichimani, A.; Sanjeeviraja, C. Preparation and characterization of PVA complexed with amino acid, proline. *Ionics* **2015**, *21* (2), 387−399.
(29) Barth, A. The infrared absorption of amino acid side chains. *Prog. Biophys. Mol. Biol.* **2000**, *74* (3−5), 141−173. From NLM Medline.
(30) Freedman, H. H. Intramolecular H-bonds. I. A spectroscopic study of the hydrogen bond between hydroxyl and nitrogen. *J. Am. Chem. Soc.* **1961**, *83* (13), 2900−2905.
(31) Peng, D. D.; Wang, S. F.; Tian, Z. Z.; Wu, X. Y.; Wu, Y. Z.; Wu, H.; Xin, Q. P.; Chen, J. F.; Cao, X. Z.; Jiang, Z. Y. Facilitated transport membranes by incorporating graphene nanosheets with high zinc ion loading for enhanced CO2 separation. *J. Membr. Sci.* **2017**, *522*, 351−362. (31a) Huang, J.; Zou, J.; Ho, W. S. W. Carbon dioxide capture using a CO2-selective facilitated transport membrane. *Ind. Eng. Chem. Res.* **2008**, *47* (4), 1261−1267.
(32) Tong, Z.; Ho, W. S. W. Facilitated transport membranes for CO2 separation and capture. *Sep. Sci. Technol.* **2017**, *52* (2), 156−167.
(33) Chen, Y.; Zhao, L.; Wang, B.; Dutta, P.; Ho, W. W. Amine-containing polymer/zeolite Y composite membranes for CO2/N2 separation. *J. Membr. Sci.* **2016**, *497*, 21−28.
(34) Hirokawa, T.; Gojo, T.; Kiso, Y. Isotachophoretic determination of mobility and pKa by means of computer simulation. IV. Evaluation of m0 and pKa of twenty-six amino acids and assessment of the separability. *J. Chromatogr.* **1986**, *369* (1), 59−81. From NLM Medline.

(35) Janakiram, S.; Lindbråthen, A.; Ansaloni, L.; Peters, T.; Deng, L. Two-stage membrane cascades for post-combustion CO2 capture using facilitated transport membranes: Importance on sequence of membrane types. *Int. J. Greenhouse Gas Control* **2022**, *119*, No. 103698.
(36) Hong, C. H.; Ahmad, N. N. R.; Leo, C. P.; Ahmad, A. L.; Mohammad, A. W. Progress in polyvinyl alcohol membranes with facilitated transport properties for carbon capture. *J. Environ. Chem. Eng.* **2021**, *9* (6), No. 106783. ARTN 106783
(37) Mulder, M.; Mulder, J. *Basic Principles of Membrane Technology*; Springer Science & Business Media, 1996.
(38) Han, Y.; Wu, D.; Ho, W. W. Simultaneous effects of temperature and vacuum and feed pressures on facilitated transport membrane for CO2/N2 separation. *J. Membr. Sci.* **2019**, *573*, 476−484.
(39) Lin, H.; Van Wagner, E.; Freeman, B. D.; Toy, L. G.; Gupta, R. P. Plasticization-enhanced hydrogen purification using polymeric membranes. *Science* **2006**, *311* (5761), 639−642. From NLM PubMed-not-MEDLINE.
(40) Yang, Y.; Han, Y.; Pang, R.; Ho, W. S. W. Amine-Containing Membranes with Functionalized Multi-Walled Carbon Nanotubes for CO2/H2 Separation. *Membranes* **2020**, *10* (11), 333. From NLM PubMed-not-MEDLINE. (40a) Zhao, Y. N.; Ho, W. S. W. Steric hindrance effect on amine demonstrated in solid polymer membranes for CO2 transport. *J. Membr. Sci.* **2012**, *415-416*, 132−138. (40b) Tong, Z.; Ho, W. S. W. New sterically hindered polyvinylamine membranes for CO2 separation and capture. *J. Membr. Sci.* **2017**, *543*, 202−211.

https://doi.org/10.1021/acs.iecr.3c02400
Ind. Eng. Chem. Res. 2023, 62, 15202−15211